Beach morphodynamic classification using high-resolution nearshore bathymetry and process-based wave modelling

D.W.T. Jackson [a,d,*], A.D. Short [b], C. Loureiro [c,d], J.A.G. Cooper [a,d]

[a] School of Geography and Environmental Sciences, Ulster University, Coleraine, Co. Londonderry, Northern Ireland, BT52 1SA, UK
[b] School of Geosciences, University of Sydney, NSW, 2006, Australia
[c] Biological and Environmental Sciences, Faculty of Natural Sciences, University of Stirling, Stirling, Scotland, FK9 4LA, UK
[d] Geological Sciences, University of KwaZulu-Natal, Durban, 4041, South Africa

ABSTRACT

Classification of beach morphodynamic state relies on accurate representation of breaking wave conditions, H_b (plus grain size and spring tidal range). Measured breaking wave data, however, are absent from all but a handful of sites worldwide. Here, we apply process-based wave modelling for propagating offshore waves to the breaking zone using high-resolution nearshore bathymetry, obtaining representative and accurate H_b values for multiple beaches at regional scale, and thereby derive meaningful morphodynamic classifications that accord with observed beach state. Ninety-five beaches on the north coast of Ireland were investigated, with observed beach types and states compared to predictions based on morphodynamic parameters determined using wave, tide and sediment data, obtained from field surveys and detailed numerical wave modelling. The coast is exposed to micro-through meso-tides (0.43–3.90 m) and low sea through high swell waves (H_b = 0.13–1.18 m) and is composed of fine to medium sand resulting in a full range of beach types (wave-dominated, tide-modified and tide-dominated) and most beach states, thereby providing a comprehensive field laboratory to undertake such a comparison. We found that modal beach types reside within their predicted Relative Tide Range (RTR) and modal beach states close to the predicted dimensionless fall velocity (Ω) range. The use of high-resolution nearshore wave modelling to determine H_b was deemed the most appropriate approach for deriving predicted beach classification. The work follows the investigation of the same coast by Jackson et al. (2005) who found shortcomings in relating beach types to breaker wave conditions. However, advances in inshore wave modelling and access to high-resolution nearshore bathymetry since then have enabled improved estimates of breaker height, producing more accurate results and enhancing previous work. The results highlight the need to obtain accurate estimates of H_b and T_p if they are to be used effectively in predicting beach parameters. This work therefore sets a precedence for other coastal sites worldwide where detailed nearshore bathymetry is available and H_b can be derived from process-based wave modelling, improving the classification and prediction of morphodynamic beach type and state.

1. Introduction

Beach systems are a product of waves and tides acting on sediment at the coast, and can be empirically characterised using four key parameters, breaker wave height (H_b) and peak period (T_p), spring tide range (TR) and sediment size (c.f. Anthony, 1998; Levoy et al., 2000; Jackson and Short, 2020). As the first three of these parameters change with time, beaches also undergo temporal change through the tidal cycle and particularly as wave conditions vary. As a consequence, beaches are in a continual state of flux as they attempt to adjust to these changes and achieve a dynamic equilibrium (Wright et al., 1985). Beach morphology responds to changes in ambient conditions and a dynamic equilibrium exists between the two, with the nature of morphological change controlled by both the ambient conditions and antecedent beach morphology (Wright and Short, 1984; Masselink and Short, 1993).

While these four parameters are widely regarded as key controls of beach morphology, each plays a particular role through time and space. Beach sediment, usually sand but ranging from fine sand to boulders, is a passive but essential component of the system, with beach gradient (and consequently width) being directly related to sediment size (c.f.

Sunamura, 1984). For a given H_b coarse-grained beaches tend to be steeper (more reflective), while fine sand beaches tend to have lower gradients (more dissipative). Beach sediment usually undergoes little temporal change in size and composition at event to decadal temporal scales, and consequently it contributes more commonly to spatial, rather than temporal variation in beach character. The vertical tidal range plays a critical role in the morphological character of a beach, with increasing range leading to a dislocation and increasing separation between the usually steeper high tide beach and lower gradient intertidal and low tide beach, surf and shoaling zone. Once the morphology has adjusted to the tide range, tides continue to play a major role in beach dynamics as the shoaling, surf and swash zone shift with the tide stage (Masselink and Short, 1993), but this is then subordinate to the role played by waves. Like grain size, tides contribute more to spatial than temporal beach change. This leaves waves as *the* most important driver of morphological change for all wave-dominated and most tide-influenced beaches, particularly via changes in wave height and direction and to a lesser extent, wave period. The importance of wave height as a driver of beach change is outlined by its contribution to the energy flux or power of waves, given that wave power (P) can be approximated as:

$$P = (\rho g^2/64\prod) \, (H_s^2 T_p) \, \text{kw m}^{-1}$$

and therefore it is the product of the square of significant wave height (H_s) and T_p (Komar, 1998; Ruessink et al., 2000), resulting in H_s being the major contributor to power and change, while T_p plays an important but secondary role, and where ρ is water density, g the gravitational acceleration.

Increases in H_b tend to lead to subaerial beach erosion and seaward sediment transport, whilst decreases lead to a slower onshore transport and beach accretion. Wave period influences these changes by positively contributing to wave power, the water depth to which wave-induced sediment transport extends, and also through its role in determining the length of standing and edge waves.

The four parameters H_b, T_p, TR and sediment size, have been used to predict both beach type and state (see Short, 2020 for a review). Beach types are defined as wave-dominated (WD), tide-modified (TM) or tide-dominated (TD) based on the relative tide range (RTR = TR/H_b). They are further classified into one of 13 beach states using the dimensionless fall velocity ($\Omega = H_b/T_p W_s$), where W_s is the sediment fall velocity (m s^{-1}). While beach type is determined by modal H_b and TR, with most beaches residing permanently in one of the three types, beach state can be in a continual state of flux, owing to changing H_b and T_p. It is therefore critical to have accurate estimates of these parameters both to understand the modal beach type and ongoing changes in beach behaviour and possibly state.

Storm events can drive major changes in beach state, with high waves lowering the beach gradient and transporting sediment seaward causing WD and TM beaches to change towards the more dissipative states, while TD beaches are more likely to be overwashed by storm waves with lesser impact on inter and sub-tidal morphology. Likewise, predicted changes in climate, in particular wave climate leading to changes in H_b, wave direction and possibly frequency and intensity of storm events, as well as TR under rising sea levels, could also drive predictable changes in modal beach state and possibly even beach type.

It is therefore critical to have accurate measurements of H_b and T_p if wave statistics are to be used for assessing beach type/state or predicting beach change. Until recently most measurements of wave height have relied on localised regional measurements of *deepwater* wave height (H_o) from wave buoys or similar stations and more recently using global and regional hindcast models (e.g., Dee et al., 2011; Perez et al., 2017). H_b has usually been measured in the field over short periods of time (hours to days), estimated visually or computed using simple approximations that disregard important nearshore wave transformation processes such as bottom friction dissipation, or assume idealized regular bathymetric

contours (e.g., Komar and Gaighan, 1972; Larson et al., 2010). However, the development of shallow water wave models such as Simulating Waves Nearshore (SWAN) (Booij et al., 1996), alongside increasingly detailed bathymetric information for nearshore areas derived from improved multibeam echo-sounding instrumentation, airborne laser technology and satellite-derived bathymetry (e.g., Pacheco et al., 2015; Caballero and Stumpf, 2021), allow more accurate estimates of H_b and T_p based on measured or modelled deep water wave parameters (Guisado-Pintado, 2020).

The aims of this paper are to, 1) to observe the range of beach types and states that occur around the dynamically diverse north coast of Ireland (n = 95); 2) to assess the contribution of TR and sediment size to each beach's state; 3) to compare the *observed* beach state with *predicted* beach state based on detailed numerical wave modelling of H_b in a subset of 29 beaches where high resolution nearshore bathymetry is available; 4) to reclassify northern Irish beaches according to revised classifications of beach type and state (Short, 2020), utilising the high-resolution nearshore bathymetric data and improved modelling of nearshore wave and tides; and in doing so 5) integrate of the Short (2006) and Scott et al. (2011) models of beach types/states into a more overarching model.

This paper is also a contribution to the increasing refinement of morphodynamic beach type/state models. Such models are required to provide a framework within which to conduct beach processes research and in some cases, to locate where a beach belongs, based either on its morphology or the relevant environmental parameters (H_b, T_p, TR and sediment). Furthermore, disequilibrium-based models developed to predict beach response to changing wave conditions also utilise these parameters to determine shoreline movement and morphodynamic states as beaches erode and/or accrete (e.g. Wright et al., 1985; Davidson et al., 2010). Such models not only allow contemporary beach change to be simulated but can also be used to predict the likely behaviour of beaches due to changes in wave climate.

2. Study area

The study area extends around the 700 km northern coast of Ireland and includes counties Sligo and Donegal in northwest Ireland and all coastal counties (Londonderry, Antrim and Down) in Northern Ireland, with a total arc located between 54 and 55.5°N (Fig. 1). The coast has a range of coastal typologies with a highly irregular and crenulated form, largely dominated by headland-bay configurations. It contains a spectrum of coastal types including rocky open coast, bays, estuaries, raised shorelines and drowned valleys, partitioning into sea cliffs, embayed sandy to gravel/cobble beaches, dunes, machair, salt marshes, wetlands and mudflats (Sinnot and Devoy, 1992; Cooper, 2007, 2010).

The coast is exposed to the North Atlantic Ocean in the northwest and north, the 20–50 km wide North Channel along the northeast coast and the fetch-limited Irish Sea in the east. The coast therefore has a gradient between two contrasting wave regimes, from the energetic North Atlantic to the relatively protected Irish Sea (Fig. 1b). Low pressure systems in the North Atlantic Ocean generate some of the highest waves in the world, particularly during the winter months (Gallagher et al., 2014), during which extreme storms frequently impact the northwest coast of Ireland (Loureiro and Cooper, 2020). Westerly Atlantic swell with annual H_s (*significant* deep-water wave height) averaging 3 m dominates the west coast, gradually decreasing in height and becoming more northwesterly along the northwest to north coasts. Waves are highest during the autumn/winter months (September to February) when H_s reaches close to 5 m, decreasing to 1–2 m during summer, while T_p average from 9 to 10 s. Closer to shore, the coastal islands and the heavily indented nature of the west and north coast induce significant wave refraction and attenuation within the bays and inlets and consequently a highly variable breaker wave regime. On the east coast, southerly winds in the Irish Sea generate local wind waves which provide more than 60% of the wave energy that reaches the coast,
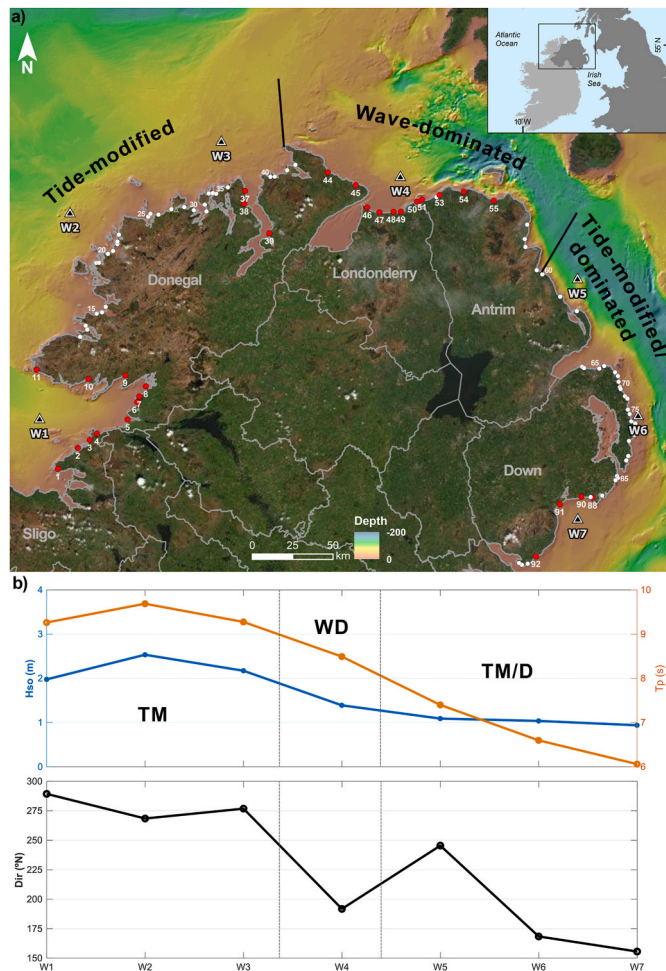
Fig. 1. a) The north coast and shelf of Ireland showing the shelf morphology and depth and location of the 95 sampled beaches and general regions of wave-dominated and tide-modified and dominated beaches. Red numbers indicate locations of modelled breaker wave height (H_b), and triangles the seven UK Met Office wave (hindcast) points utilised in the study (W1-7). **b)** Average deep-water wave height (H_o) and period (T_p) and direction at each of the seven hindcast locations. Bathymetric data from EMODnet Bathymetry Consortium (2018).

Fig. 2. Plot of co-tidal (Mean Spring) range contours (m) around the north coast of Ireland. Output based on POLPRED2 tidal model by Proudman Oceanographic Laboratory operating over a spatial high resolution and a 5-year time-series between 2003 and 2008.

2020), including a series of sites around the northern Irish coast (Jackson and Cooper, 2009a). Jackson et al. (2005), in the absence of any detailed bathymetry and nearshore wave modelling, used the Komar and Gaighan (1972) formula to predict H_b. This produced abnormally high values for H_b and consequently lower RTR and higher Ω, which resulted in the disagreement between predicted and observed beach types and states. In this paper, we also take a regional approach to beach morphodynamics along the same coast, investigating 95 sandy beach systems (Fig. 1a) that vary markedly in wave exposure and tidal range, and are representative of the considerable local variation in H_b and TR around the coast (Orford, 1989). However, with the benefit of high-resolution nearshore bathymetry and numerical wave modelling, we are now able to produce more detailed and realistic estimates of H_b and T_p.

3. Methods

Considering the wide range of wave, tide and sediment characteristics, as well as geomorphological setting of beaches along the northern coast of Ireland, a detailed evaluation of the environmental conditions and dynamic forcing was implemented to assess beach morphodynamic characteristics. This was achieved by integrating high-resolution wave and tide modelling, detailed grain-size analysis and comprehensive evaluation of modal beach type and state.

3.1. Sediment sampling and analysis

Sediment samples were collected from the most energetic part of the beach which varies with type and state. For wave-dominated dissipative and intermediate beaches sand was collected from the surf zone, on reflective beaches from the mid swash zone and on all tide-modified and tide-dominated beaches from the intertidal zone below the high tide beach. Sediment fall velocity was obtained using a settling tube, with sediment size derived by measuring settling velocity of sand particles in water as they fall through a water column and converting these to a grain size equivalent. This method, described fully in Flemming and Thum (1978), offers a finer resolution than sieving and is thought to better represent natural hydraulic settling behaviour of the sediment collected on each beach.

with annual H_s less than 1 m and never exceeding 2 m, with periods decreasing to 6 s. Wave direction also rotates from west-northwest (290°) in the west, varying between 190 and 270° along the north coast due to wave refraction, changing to southeast (150°) in the Irish Sea (Fig. 1b).

The mean spring tidal range around the north coast varies from meso-tidal (2–4 m) in counties Sligo and Donegal, reducing to micro-tidal (<2 m) in counties Londonderry/Antrim, while along the County Down coast the tide increases from micro in the north to just macro-tidal (4 m) in the south (Fig. 2).

Previous studies of beach morphodynamics in the region have focussed largely on specific sites such as Five Finger Strand, Co. Donegal (Cooper, et al., 2006; Jackson et al., 2016; Guisado-Pintado and Jackson, 2018, 2019), Magilligan Point, Co. Londonderry (Carter, 1975, 1979, 1980a,b, 1986, 1988, 1991; Carter et al., 1982; Carter and Stone, 1989; Anfuso et al., 2020), Runkerry beach (Shaw 1985; Huang et al., 2002), the southeast (Co. Down) coast of Northern Ireland on the Ards Peninsula (Bowden and Orford, 1984) and Dundrum Bay (Cooper and Navas, 2004; Biausque et al., 2021). Jackson et al. (2005) presented a regional comparison of beach states that included 25 beaches and explored aspects of geological control (Jackson and Cooper, 2009b; Gallop et al.,
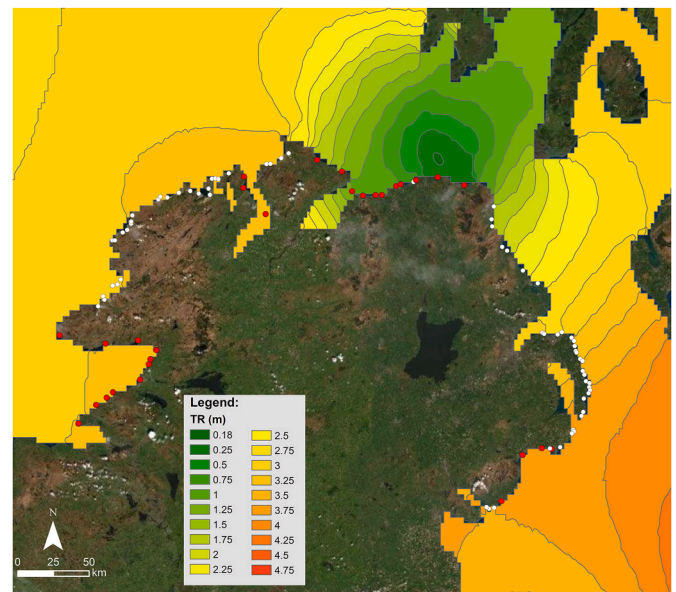
3.2. Tide modelling

Mean spring tidal range at each beach site was calculated using the high resolution (cell size 1.3 km × 2.3 km) POLPRED2 tidal prediction model (Proudman Oceanographic Laboratory, 2004) (Fig. 2). Model tidal predictions are derived for a particular location from a set of harmonic constants which have been interpolated from harmonic constants of four surrounding grid squares. Its reference datum is an 'undisturbed sea surface' parallel to the geoid.

3.3. Breaking wave modelling

Accurate estimates of H_b are critical in the prediction of RTR, Ω and beach state. Given the complex bathymetric configuration of the continental shelf and shoreface around the north coast of Ireland and the importance of detailed nearshore characterisation for accurately modelling depth-induced breaking waves, high-resolution bathymetric grids were only available for 29 beaches that had complete bathymetric coverage, which allowed detailed modelling of wave breaking (red points in Fig. 1). Consequently, wave height was only modelled for a subset of the 29 beaches (of the 95) where suitable nearshore bathymetry was available. At these locations H_b and T_p were derived from nearshore propagation of offshore waves for a period of 5 years between 2003 and 2008, using a high-resolution implementation of the spectral wave model SWAN (Booij et al., 1999; Ris et al., 1999). Offshore waves were obtained in deep (102 m) to intermediate (25 m) water depths from the Met Office UK Waters Wave Model hindcast data (Saulter, 2009) for the seven locations around the north coast of Ireland identified in Fig. 1.

Rectilinear grids with a resolution of 10 m were produced for each location using multi-beam swath bathymetric data collected along different sections of the north coast of Ireland in the framework of the INFOMAR/INSS (Integrated Mapping for the Sustainable Development of Ireland's Marine Resource/Irish National Seabed Survey) program, the JIBS (Joint Irish Bathymetric Survey) initiative, as well as multi-beam data made available through the UK Hydrographic Office INSPIRE Portal. In some locations, where shallow multi-beam coverage was limited, the bathymetry for areas shallower than 10 m depth was supplemented with satellite-derived nearshore bathymetry using a depth-inversion algorithm based on multiple linear regression (Pacheco et al., 2015), calibrated with bathymetric data from adjacent areas with complete multi-beam coverage. Root mean square errors (RMSE) for the satellite-derived nearshore bathymetry range between 0.5 and 1.5 m, with RMSE values higher than 1 m observed in areas deeper than 6 m and with increased turbidity. All bathymetric grids were adjusted to mean sea level using the UK Hydrographic Office Vertical Offshore Reference Frame (VORF) model (Turner et al., 2010).

SWAN was implemented in third generation, 2D stationary mode, using a JONSWAP spectral shape to represent the wave field, directional discretization in regular classes of 10° and frequency discretization in 30 logarithmic distributed classes between 1 and 0.03 Hz. Following Loureiro et al. (2012) and Matias et al. (2019), SWAN runs were performed using default parameters for white capping dissipation, non-linear triad wave-wave interactions as they are highly significant in shallow coastal areas (Booij et al., 1999; Holthuijsen, 2007), bottom friction dissipation according to the default variable JONSWAP expression of Hasselmann et al. (1973). Depth-induced breaking was determined according to the β-kd model for surf-breaking (Salmon and Holthuijsen, 2015).

Stationary runs in SWAN simulate the instantaneous propagation of waves based on input boundary conditions obtained from offshore parametric wave data, instead of wave generation due to wind forcing. For determining modal breaking wave conditions, the sub-daily variability was disregarded, and the simulations with SWAN were run with a daily time step for a period of 5 years, using the average daily parametric wave data (H_s, T_p and direction) from the seven Met Office wave model grid nodes as input for the offshore boundary conditions. Rectilinear computational domains with a resolution of 10 m, extending from the location of the offshore wave forcing to the shoreline of each beach were used in all model runs.

SWAN simulations provided detailed representation of the nearshore wave field in each of the 29 beaches where wave modelling was implemented, and model outputs were analysed to determine breaking location and extract H_b and associated T_p. Breaking location was determined using the modelled fraction of breaking waves due to depth-induced breaking, assigning breaking location to the most offshore cell where this value exceeds 1% (Harley et al., 2007). Following Loureiro et al. (2013), daily H_b and associated T_p for each beach were computed by alongshore averaging of the values of these parameters in the cells fronting the beach that matched the breaking location in each model run. Sections where averaging was computed were centred on the middle of the beach and ranged from 300 m to 2500 m, depending on the beach length.

3.4. Observed beach states

All 95 beaches were inspected between 23.07 and 13.08 2007 and again between 18.09 and 7.10.2013, during which time the beach type/state was noted and sediment samples collected from the appropriate cross-shore location. Beach state was determined by visual observations of the beach at low tide. As these inspections represented just one or two temporal samples, a range of imagery was inspected to determined beach state at the time of image capture. These include Google Earth imagery over various years for the entire coast, GeoHive aerial photomosaics for 1995, 2005, 2020 and Premium and Digital Global 2011–2013 of the Irish coast, and Ordnance Survey of Northern Ireland aerial mosaics of the Northern Ireland coast. This provided six aerial image sequences for the northwest coast of Ireland but only one for the Northern Ireland coast. When combined with the results of the field investigations and repetitive Google Earth imagery they provide a reasonable temporal sample of each beach's state and variability. Most beaches showed minimal variability with many of the beaches exhibiting surficial changes but no change in state, as is typical of TM, TD and dissipative WD beaches when compared to intermediate and reflective WD beaches.

Fig. 3a plots the region of WD, TM and TD beach types and the modal locations of each of the 13 beach states relative to TR and Ω based on micro through mega-tidal Australian beaches, while Fig. 3b plots ten beach states based on predominantly large tide range UK beaches some of which are also separated into high (HE) and low energy (LE) beach states. The lower table (Fig. 3c) correlates the two classification schemes which have considerable overlap. Combined these schemes account for most of the world's beach types/states. A fuller description of each of the beach types and states can be found in Short (1999, 2020), Scott, et al. (2011) and Short and Jackson (2013).

It must be noted that the above model is for single bar WD beaches as well as the double bar dissipative end member together with the TM and TD beaches. Models of double and multi-bar behaviour have been proposed by Short (1992), Short and Aagaard (1993), Castelle et al. (2007) and Price et al. (2014), all of which present increasingly refined models of wave-dominated double/multi-bar systems. These models are not considered in Fig. 3 nor in this study, as there are no double bar systems in the study area. Hegge et al. (1996) did propose a low energy model for 'sheltered' wave-dominated beaches, which might be expected to relate to the east coast, lower energy tide-modified beaches. However, the Western Australian beaches they studied were all in micro-tidal environments, exposed to low, though long period swell, a marked contrast to the meso-tidal, fetch-limited east coast beaches and consequently display markedly different morphologies. Likewise, Gallop et al. (2020) developed longshore and cross-shore models of geological controlled beaches. The longshore model focuses on the degree of beach embaymentisation that controls nearshore circulation, while the cross-shore model considers the degree to which bedrock truncates the dynamic
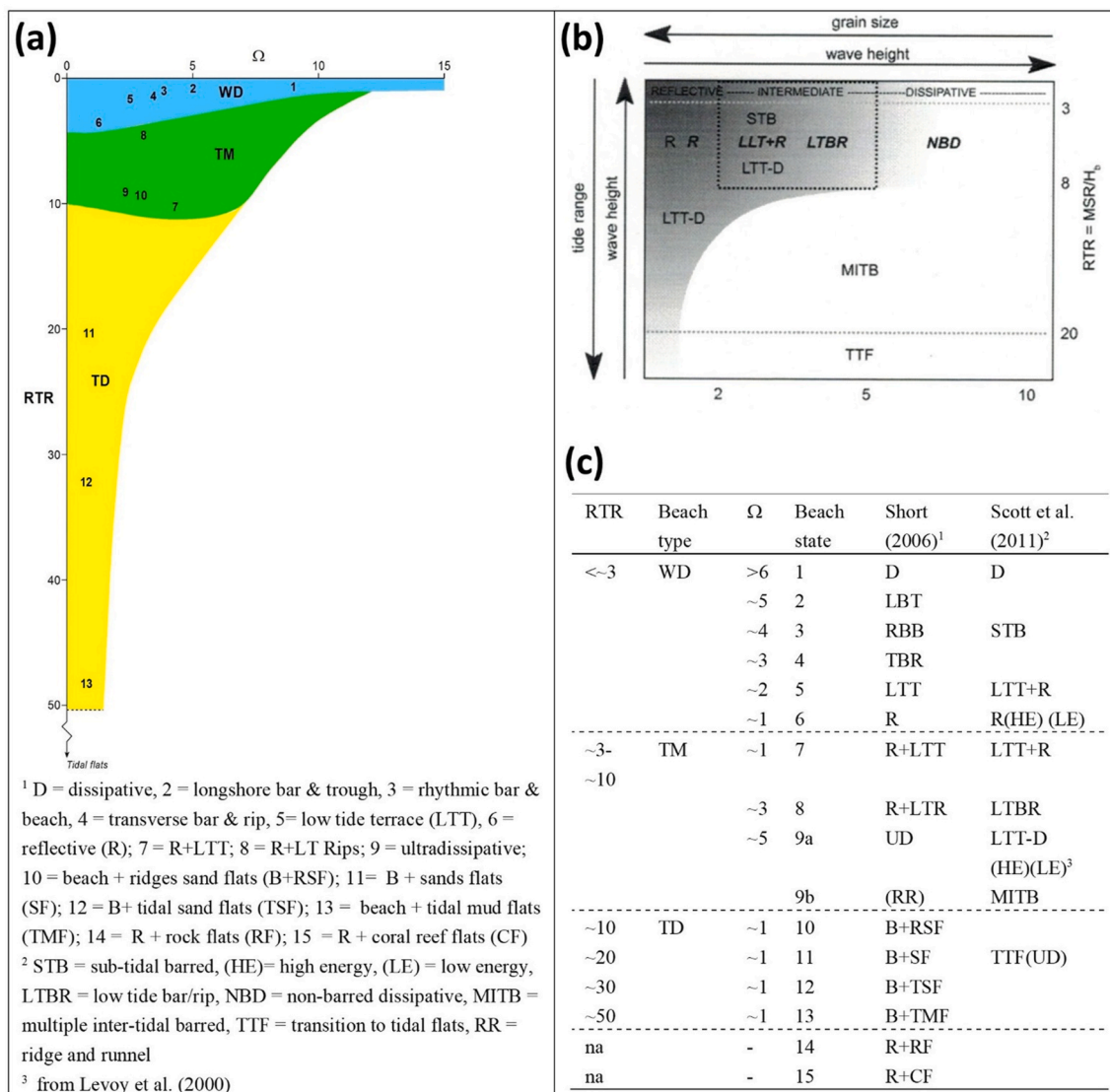
Fig. 3. a) Relationship between Ω and RTR in controlling Australian beach type and state (WD=Wave-Dominated, TM = Tide-Modified, TD = Tide-Dominated) (source: Short and Jackson, 2013). Numbers refer to the mean location of WD (beach states 1–6), TM (7–9) and TD (10–13) beach states; **b)** similar diagram from Scott et al. (2011) based on UK beaches; and **c)** table correlating beach type and state between the two approaches (Modified from Short, 2020). Note, apart from dissipative beaches, the WD related to single bar beaches and the boundaries between beach types are not rigid.

equilibrium profile of the beach. In this study, geological control was involved to the degree it affected the breaker wave regime through wave sheltering, attenuation and refraction and consequently beach characteristics, but not how it influenced the shape and mobility of the beach profile.

3.5. Predicted beach states

In order to properly use the empirical RTR and Ω parameters it is essential to have accurate measures of TR, H_b, T_p and W_s. Predicted H_b and T_p were obtained using SWAN to model the nearshore wave conditions for the subset of 29 beaches where high-resolution bathymetry was available to allow prediction of both. The predicted H_b and T_p were then combined with the W_s measured using the beach sediment samples and mean spring TR obtained using the POLPRED2 model to calculate RTR and Ω for each beach (Table 1). Where complete nearshore bathymetry was unavailable then those beach sites were not examined for beach state prediction. Although improved wave hindcasts produced by the Met Office for the Copernicus Marine Service are now available for the NW European shelf, the 1.5 km resolution of such regional wave

models, implemented using coarse bathymetric grids and simplified shoreline representation prevent their use for determining breaking wave parameters at the sub-grid spatial scale typical of most beaches. Moreover, while such hindcasts can provide more detailed characterisation of offshore wave conditions, their propagation to individual beaches using parametric approaches for refraction and shoaling without detailed bathymetric information, would render estimates of breaking wave height too uncertain in coastal areas characterised by complex nearshore bathymetry.

4. Results

4.1. Observed beach states

The 95 beaches in the study provide a representative sample of the beach systems of Ireland's north coast, ranging from WD though TM to TD (Table 1; Fig. 4). The beaches are exposed to H_s ranging from 2.5 to 1 m, T_p between 6 and 7 s (Fig. 1b), H_b between 0.45 and 1.11 m (Table 1), micro through high meso-tidal ranges (0.43–3.89 m) (Fig. 2), with beach sediment predominately composed of quartz sand which grades from

Table 1

The 95 beaches and their characteristics of which 92 were used in the study and the 29 in italics selected for SWAN modelling of H_b and T_p, (BS- beach state).

	Donegal	Spring Tide (m)	H_b	T_p	mean (mm)	fall vel (ms^{-1})	RTR	Ω	Mean BS
1	*Raghly*	*3.26*	*1.11*	*7.30*	*0.137*	*0.034*	*2.93*	*4.43*	*7.3*
2	*Streedagh*	*3.26*	*1.05*	*7.21*	*0.201*	*0.030*	*3.10*	*4.81*	*7.6*
3	*Cliffony*	*3.27*	*1.18*	*7.25*	*0.211*	*0.033*	*2.77*	*4.88*	*7.7*
4	*Mullaghmore*	*3.28*	*0.44*	*7.05*	*0.190*	*0.020*	*7.45*	*3.20*	*7.4*
5	*Tullan Strand*	*3.33*	*1.06*	*7.32*	*0.176*	*0.028*	*3.14*	*5.12*	*8.1*
6	*Rossnowlagh*	*3.34*	*0.85*	*7.17*	*0.140*	*0.029*	*3.93*	*4.10*	*8.8*
7	*Inishinny*	*3.35*	*0.51*	*6.69*	*0.140*	*0.025*	*6.57*	*3.10*	*9.0*
8	*Murvagh Strand*	*3.35*	*0.44*	*4.97*	*0.190*	*0.029*	*7.61*	*3.01*	*9.0*
9	*Inver*	*3.34*	*0.16*	*6.00*	*0.176*	*0.028*	*20.88*	*0.96*	*10.8*
10	*Fintra*	*3.26*	*0.39*	*6.56*	*0.198*	*0.036*	*8.36*	*1.67*	*9.1*
11	*Malin Beg*	*3.19*	*0.39*	*7.09*	*0.298*	*0.061*	*8.18*	*0.90*	*6.7*
12	Maghery Strand	3.19			0.230	0.040			
13	Loughros More (S)	3.21							
14	Tramore Beach	3.20			0.190	0.031			9.0
15	Naran (or Narin)?	3.23			0.180	0.026			7.8
16	Lettermacward (N)	3.25			0.130	0.015			7.4
17	Dooey	3.25			0.210	0.033			9.0
18	Illancarragh (W)	3.21			0.393	0.116			6.4
19	Illancarragh (E)	3.22			0.321	0.077			6.9
20	Mullaghderg	3.23			0.666	0.333			7.4
21	Carrickfin Beach	3.25			0.170	0.050			7.4
22	Bunbeg (S)	3.26			0.418	0.131			11.0
23	Derrybeg	3.26			0.310	0.072			11.0
24	Lunniagh	3.26			0.351	0.092			7.0
25	Magheraroarty	3.36			0.170	0.026			7.4
26	Ballyness (E)	3.36			0.516	0.200			7.4
27	Falcarragh (E of Magheraroarty)	3.36			0.200	0.030			7.9
28	Tamore Beach	3.37			0.180	0.025			7.9
29	Dunfanaghy	3.38			0.170	0.027			7.0
30	Marblehill	3.38			0.140	0.025			7.0
31	Tra Mor	3.39			0.130	0.015			7.8
32	Downings	3.39			0.277	0.058			7.0
33	Rosguil/Tranrossan	3.39			0.366	0.100			7.6
34	Mulroy Bay (W)	3.39			0.355	0.094			11.1
35	Mulroy Bay (E)	3.40							10.3
36	Ballyhiernon	3.40			0.190	0.015			7.6
37	*Doagh Beg (S)*	*3.41*	*0.58*	*7.16*	*0.270*	*0.057*	*5.88*	*1.42*	*6.9*
38	*Stocker Strand*	*3.42*	*0.32*	*7.37*	*0.210*	*0.032*	*10.69*	*1.38*	*7.0*
39	*Fahan*	*3.45*	*0.13*	*7.42*	*0.245*	*0.045*	*26.52*	*0.39*	*11.2*
40	Rockstown Bay	3.37			0.224	0.038			6.2
41	Tullagh Bay	3.37			0.190	0.031			6.9
42	Pollen Strand	3.31			0.210	0.032			7.9
43	Five Finger	3.05							
44	*Culdaff*	*1.90*	*0.78*	*5.21*	*0.140*	*0.015*	*2.43*	*10.19*	*5.5*
45	*Kinnego Bay*	*1.57*	*0.73*	*5.00*	*0.350*	*0.111*	*2.44*	*1.23*	*6.0*
46	*Magilligan*	*1.24*	*0.58*	*6.35*	*0.190*	*0.027*	*2.15*	*3.37*	*4.0*
47	*Benone*	*1.21*	*0.68*	*6.56*	*0.157*	*0.018*	*2.14*	*5.61*	*4.5*
48	*Castlerock*	*1.19*	*0.70*	*6.73*	*0.166*	*0.021*	*1.78*	*5.03*	*4.5*
49	*Portstewart*	*1.20*	*0.64*	*6.75*	*0.157*	*0.018*	*1.70*	*5.13*	*4.5*
50	*Portrush (W)*	*1.15*	*0.61*	*6.64*	*0.186*	*0.026*	*1.88*	*2.61*	*4.8*
51	*Portrush (E)*	*0.99*	*0.45*	*6.67*	*0.197*	*0.029*	*2.56*	*2.27*	*4.8*
52	Portballintrae	0.78							6.0
53	*Runkerry*	*0.80*	*0.63*	*6.73*	*0.280*	*0.059*	*0.64*	*1.59*	*4.1*
54	*White Park Bay*	*0.46*	*0.72*	*6.63*	*0.229*	*0.039*	*0.70*	*2.76*	*3.7*
55	*Ballycastle*	*0.43*	*0.61*	*6.27*	*0.634*	*0.301*	*11.81*	*0.32*	*4.0*
56	Cushendun	1.89			0.397	0.118			4.5
57	Cushendall	1.87			0.296	0.066			4.5
58	Red Bay/Waterfoot	1.88			0.169	0.021			5.0
59	Carnlough	2.13			0.193	0.028			5.2
60	Glenarm	2.21			0.205	0.032			7.0
61	Ballygalley	2.43			0.218	0.036			7.0
62	Browns Bay	2.64			0.210	0.033			7.0
63	St Helens Bay (N)	3.01			0.248	0.046			7.0
64	St Helens Bay (S)	3.01			0.370	0.103			7.0
65	Ballyholme Bay	2.99			0.683	0.350			11.0
66	Groomsport Bay	2.98			0.290	0.063			9.0
67	Sandy Bay	3.19			0.251	0.047			9.0
68	Donaghaee Harbour	3.31			0.231	0.040			12.0
69	Ballyvester	3.35			0.245	0.045			12.2
70	Millisle (N)	3.35			0.497	0.185			12.2
71	Millisle (S)	3.41			0.186	0.026			10.7
72	Whiskin Shore	3.46			0.263	0.052			10.5
73	Ballyferris	3.48			0.190	0.027			9.0

Table 1 (*continued*)

	Donegal	Spring Tide (m)	H_b	T_p	mean (mm)	fall vel (ms^{-1})	RTR	Ω	Mean BS
74	Ballywater	3.56			0.221	0.037			10.5
75	Balliggan	3.61			0.213	0.034			10.5
76	Ballyhalbert	3.68			0.248	0.046			7.0
77	Ballyhalbert Pier	3.72			0.220	0.036			10.2
78	Portavogie (N)	3.77			0.226	0.038			11.0
79	Portavogie	3.77			0.240	0.043			10.2
80	Portavogie Bay	3.81			0.325	0.079			9.5
81	Cloughey Slipway	3.83			0.195	0.029			10.7
82	Kearney Point	3.88			0.213	0.034			8.0
83	Millin Bay	3.91			0.179	0.024			8.0
84	Quarter Bay	3.93			0.219	0.036			9.2
85	Killard Point (Benderg Bay)	3.92			0.780	0.450			8.0
86	Ballhornan	3.92			0.376	0.106			8.0
87	Conmey Island Bay	3.90			0.215	0.033			7.0
88	*Rossglass*	3.90	*0.33*	*4.53*	*0.170*	*0.024*	*11.81*	*3.06*	*10.4*
89	Minerstown (E)	3.90			0.165	0.022			8.2
90	*Tyrella*	3.90	*0.44*	*4.92*	*0.160*	*0.020*	*8.86*	*4.43*	*10.7*
91	*Murlough*	3.89	*0.41*	*5.06*	*0.150*	*0.017*	*5.98*	*7.27*	*9.0*
92	*Kilkeel*	3.77	*0.65*	*5.30*	*0.230*	*0.030*	*5.80*	*4.09*	*9.0*

fine thorough medium, with a few beaches composed of coarse sand (mean = 0.27 mm, σ = 0.14 mm) (Fig. 5).

Table 1 lists the 95 beaches and their mean observed beach state/s from the site inspections and the imagery. Each beach's state was numerically coded using the beach state numbers (1–15) in Fig. 3. Where the beach state varied through time the mean value is used in Table 1 resulting in fractional values where the mean state resides between two states. Three beaches (#12, 13 and 43) were removed from the assessment as they are strongly influenced by their position adjacent to tidal inlets. The modal (mean) beach states range from WD: R, LTT and TBR, through all three TM states: R +LTT, R+LTR and UD (RR), to the TD: B+RSF, B+SF and B+TSF. The coast is, however, dominated by TM beaches with the full range occurring in the western and eastern meso-tidal regions (Figs. 1 and 6a), with the types closely following the tide range as is to be expected (Fig. 6b). In general, the higher energy TM and WD beaches are located in the meso-tidal west to northwest (#1–44) and microtidal north to northeast (#45–59) and the predominately lower energy TM and TD beaches in the east (#60–95), with the RR representing the highest energy of these eastern TM systems. However, because of the indented nature of the coast three TD beaches also occur in sheltered west-north coast locations (#9, 22–23). The remaining TD beaches occur both on the north coast (#34, 35, 39) where they are located in sheltered embayments and consequently receiving lower waves, and down the east coast (between #65–95) where tides increase in range reaching 3.9 m as H_s decreases to 1 m and H_b to between 0.3 and 0.6 m. The mix of TM and TD beaches along the east coast can be attributed to both the tide range (3–3.9 m) and subtle variations in exposure which controls H_b, particularly as there is no significant difference in T_p or mean grain size (mean 0.245 mm for TM and 0.286 mm for TD) (Table 1 and Fig. 6c).

4.2. Predicted beach states/type

The following examines the role of Ω, RTR, TR, H_b and grain size in influencing beach type-state for the predicted states. Fig. 7 plots the observed beach state versus predicted Ω and RTR. In general, the WD beaches (BS 1–6) are all located in the lower RTR (<3), the TM (BS 7–9) between RTR 2.6–10.7, and the TD (BS 10–11) are all >10. This is in agreement with the findings of Short (2006), Scott, et al. (2011) and Short and Jackson (2013) for English, Welsh and Australian beaches and indicates that RTR is a good determinant of beach type.

Waves and tides are the prime determinant of beach type and state. While mean H_s ranges from 2.5 m in the west to 1 m in the east (Fig. 1), mean H_b has a maximum of 1.18 m at beach #3 in the west and a low of 0.33 m in the east at beach #88. These are substantially lower than the

H_b calculated for the same coast by Jackson et al. (2005), which can be attributed to the use of detailed wave modelling in the current study. The method here uses similar H_s and T_p to the work of Jackson et al. (2005) for this region, but implements high-resolution wave modelling with SWAN using complete bathymetric coverage to model detailed onshore propagation, refraction and attenuation and final derivation of H_b, providing a much more accurate estimate of H_b and consequently Ω, RTR and beach state. It should be noted that H_b determined with the empirical parameterisation of Komar and Gaighan (1972) was 4–6 times higher than SWAN-derived H_b values across sites.

As expected, the TD (beaches #9, 39, 88, 90) beaches have the lowest H_b, all <0.5 m, with the TM (beaches #1–8, 10–38, 42, 44, 91, 92) ranging from 0.5 to 1.18 m (Table 1, Fig. 8a), which is also unsurprising given the exposure of these beaches to H_s ranging from 1 to 2.5 m. The WD (beaches #45–55) beaches all occur along the microtidal north coast where H_b ranges from 0.44 to 0.73 m a result of the lower H_s (~1.5 m) coupled with wave attenuation.

Tide range, as discussed above, is closely related to beach type with all the WD beaches having <1.6 m spring tide range, the TM ranging from 1.2 to 3.9 m but predominately in the meso-tidal range (3.2–3.9 m), while the three TD beaches have tidal ranges between 3.3 and 3.9 m the highest in the study area (Table 1; Fig. 8b).

As noted above, grain size plays a secondary role in beach type being more prominent in influencing beach state within the types. Fig. 8c plots the grain size for the predicted beaches with a crude trend of finer sand associated with the WD beaches increasing slightly in size into the TM and TD beaches. This trend is more apparent in Fig. 6c.

RTR ranges from 0.64 to 26.52, with all the WD < 2.6, the TM ranging between 2.4 and 10.7, and the TD ranging from 8.9 to 26.5, all in general agreement with Short (2006) and Scott et al. (2011). There is a general east to west transition in RTR in parallel with the same transition from meso to micro to meso-macro tides and associated TM to WD beaches then to TM and TD beaches, reflecting the same transition from meso to micro to meso-macro tides. The plot of RTR versus beach state (Fig. 8d) clearly highlights its role in discriminating between beach types, with all the WD < 2.6, the TM ranging between 2.4 and 10.7, and the TD ranging from 8.9 to 26.5, all in general agreement with Short (2006) and Scott et al. (2011).

Finally, the comparison of beach state against Ω (Fig. 8e), which is largely dependent on H_b, shows a spread in all three types with the greatest spread in the more exposed higher energy TM beaches, followed by the WD and least in the perennially low energy TD beaches.

In terms of beach type as mentioned above, the three types predominately fall within the expected boundaries, with two of the TMs having an RTR of 2.8 and 2.9 lying just inside the WD boundary of ~3,

WAVE-DOMINATED

Fig. 4. Selection of surveyed sites representative of the range of beach types and states observed. Arranged high to low energy. Wave-dominated: **(A)** TBR White Park Bay (#54); **(B)** LTT Culdaff (high tide) #44; **(C)** LTT Portstewart (low tide) #49; **(D)** LTT Cushendun (cobble high tide beach) #56;**(E)** R Kinnego #45; Tide-Modified: **(F)** R+LTT St Helens Bay #63; **(G)** R+LTT Raghly #1; **(H)** R+LTR Tullan #5; **(I)** R+LTR Ballyhornan #86; **(J)** UD Rossnowlagh #6; **(K)** RR Dundrum #91; Tide-Dominated: **(L)** B+SF Tyrella #90 and **(M)** Cranfield #95 (rippled sand flats); **(N)** B+SF Ballyhalbert #77; **(O)** B+TF Cloughy (high beach with flats insert) #81.

TIDE-MODIFIED

TIDE-DOMINATED

and at the TM-TD boundary with one TM at 10.69 while a TD is 8.86 (Fig. 8d). However, as noted by Short (2006) and Scott et al. (2011), the boundaries are not fixed and expected to have some degree of flexibility depending on the regional wave-tide-sediment environment, with Short (2006) giving the TM-TD boundary as a zone between 10 and 12. Finally, the location of the beach states with respect to Ω (Fig. 7) does not show the discernible trends found by Short (2006) and Scott et al. (2011). This can in part be attributed to a smaller sample size.

5. Discussion

The northern coast of Ireland provides an ideal environment within which to examine the impact of varying wave height and tide range on sandy beach type and state over a relatively small geographical coastal stretch, and to use this variation to examine the role played by waves, tides and sediments on beach morphodynamic classification.

As Figs. 7 and 8d indicate, RTR was shown to be a good discriminator
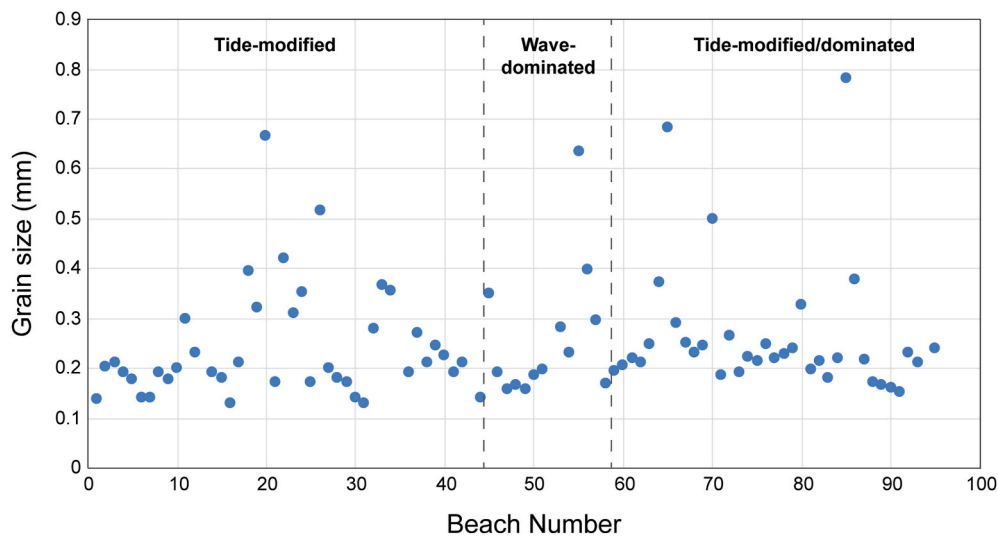
Fig. 5. Mean beach sand size (mm) for each of the 95 beaches. See Table 1 for beach names and sediment data.

of beach type with boundaries between WD and TM around 3 and between TM and TD around 10, as found by Masselink and Short (1993), Short (2006) and Scott et al. (2011). Tide range alone provides a general trend with WD beaches having spring tides generally <2 m, TM between 1 and 4 m and TD > 3 m (Fig. 8b). The overlap between beach types is due to the fact that H_b also plays and important role in determining both beach type *and* beach state. To examine the role of H_b, it was plotted against beach state which showed TD beaches receive the lowest waves ($H_b < 0.5$), while H_b in TM beaches range from 0.39 to 1.18 m, with all WD beaches $H_b > 0.44$ m (range 0.44–0.78 m) (Fig. 8a). The spread in beach states within the WD and TM beach types (Fig. 7) is driven by the fact that waves control beach states within each type. In order to examine this relation, beach state was plotted against Ω. Fig. 3a suggests there should be a trend from lower to higher energy states with increasing H_b as indicated by increasing Ω. However, as Fig. 7 indicates, this is not the case with higher and lower energy WD and TM states spread across a range of Ω values, which may in part be attributed to the small sample size. Scott et al. (2011, Figs 15 and 16) also found considerable variation in both RTR and Ω for each beach state, with the spread tending to be greater in the higher energy WD and TM states, and least in the lower energy TD states. For this reason, they, like Short (2006), do not propose clear boundaries between types and states, rather they are part of an overlapping spectrum of beach change, though modal states can be defined within each of the RTR boundaries.

Previous studies on many of the same beaches by Jackson et al. (2005) found a lack of agreement between predicted and observed beach states, attributing underlying geological control to significantly influencing beach states. This discordance however, may also be attributed to the different methods used for calculating H_b. With no adequate nearshore bathymetry available for the 2005 study (as with many beach investigations even today), they used the empirically-derived Komar and Gaighan (1972) expression:

$$H_b = 0.39 \ g^{\ 1/5}(T_pH_s^{\ 2})^{2/5}$$

This equation, while considering H_s and T_p, does *not* take account of variations in nearshore bathymetry, rather using the same correction factors to estimate H_b for all beaches, which resulted in values for H_b that exceeded the H_s, implying that no wave attenuation occurred. H_b values in Jackson et al. (2005) were consistently higher (4–6 times) than H_b modelled with SWAN. This in turn, produced predictions of higher Ω, and exceptionally low RTR values and when RTR was correlated with Ω, all the beaches were categorised as barred D owing to the high Ω and low RTR. However, in the present study, the recent availability of

high-resolution multibeam and satellite-derived nearshore bathymetry together with localised hindcasted wave parameters (Met Office UK Waters Wave Model) enabled the use of numerical wave modelling to better predict H_b at 29 sites.

Implementation of SWAN for detailed modelling of the nearshore wave field, including the complex wave refraction and attenuation that occurs in the geomorphologically complex nearshore and coastline of the north of Ireland, enabled computation of wave parameters that more realistically reflect the changes in wave characteristics as they propagate from deep and intermediate to shallow water at each beach. Additionally, the use of the β-kd model (Salmon and Holthuijsen, 2015) to determine depth-induced breaking in SWAN, allowed a dynamic scaling approach based on local bottom slope and water depth, which are the most important variables in determining wave breaking (Balsillie, 1983). The β-kd model has been shown to outperform more traditional scaling approaches (Salmon and Holthuijsen, 2015), often based on breaker indexes determined by constants or offshore wave parameters (Power, 2020), providing site-specific estimates instead of generic approximations.

While there are always limitations in constraining beach states to averaged values based on modelled parameters (Loureiro et al., 2013), use of high-resolution wave modelling for determining site-specific breaking wave parameters helped produce much more detailed (and informed) values of H_b, T_p and thereby RTR and Ω for the selected beaches in this study. The results here therefore highlight the need for accurate derivations of breaking wave parameters, which in the absence of long-term nearshore wave observations, may have to rely on high-resolution wave modelling, which in turn relies on accurate deepwater wave conditions and detailed bathymetry. This is particularly so on coasts with more complex nearshore bathymetric configuration that may significantly alter wave attenuation and energy delivery to beaches. Past studies (e.g. Jackson et al., 2005; Klein and Menezes, 2001; Pereira et al., 2016; Vital et al., 2016), have often focused on predictions of beach state and type but without the benefit of accurate methods to derive H_b. Future studies may well benefit from a similar approach taken in this study, especially if nearshore bathymetry becomes available at high resolution within and before the predominant wave breaking zone where mapping was not previously possible at sufficient resolution. Satellite-derived bathymetry offers significant potential in this area (Traganos et al., 2018; Caballero and Stumpf, 2021).

This paper is also an important contribution to the ongoing refinement of beach type/state models. Such models are required to provide a basis on which to conduct research and in some cases, to locate where a beach belongs based either on its morphological signature or the
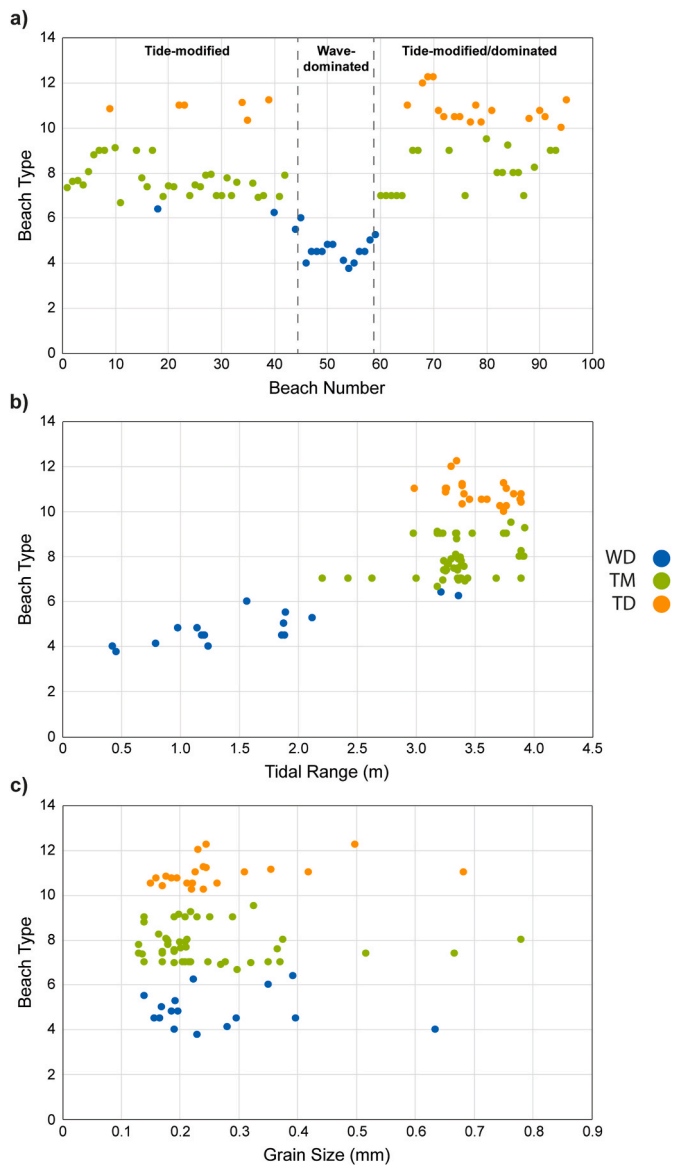
Fig. 6. a) Observed beach type for each beach; **b)** beach type versus tide range; and **c)** beach type versus grain size (see Table 1 for data) (WD = Wave-Dominated, TM = Tide-Modified, TD = Tide-Dominated).
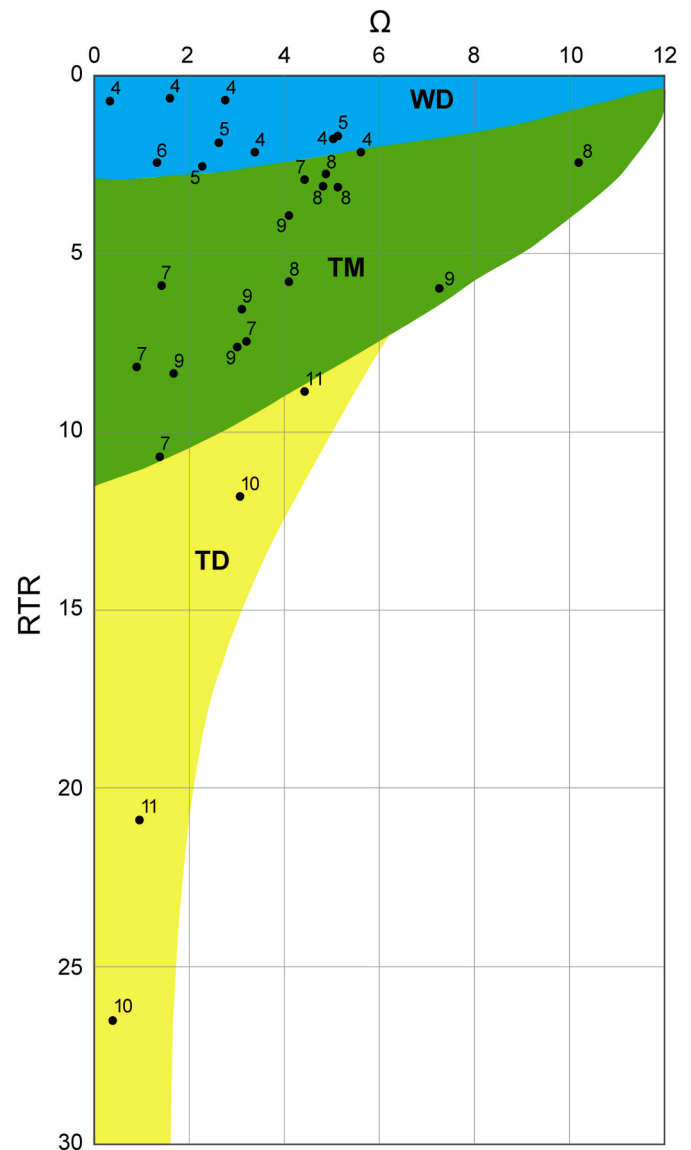

Fig. 7. Predicted Ω and RTR for the 29 selected beaches with beach state (1–11) noted for each beach and beach type domains and approximate boundaries. (WD = Wave-Dominated, TM = Tide-Modified, TD = Tide-Dominated).

relevant environmental parameters (H_b, T_p, TR and sediment). Additionally, predictive models of beach response to variable wave conditions also use these parameters to predict movement though the states as beaches erode and/or accrete (e.g. Wright et al., 1985; and Davidson et al., 2010) and may in future help predict beach response to climate-induced changes in wave climate and tide range.

Finally, this paper has attempted to use field data to integrate the Short and Jackson (2013), Scott, et al. (2011) and Short (2020) sequential beach models illustrated in Fig. 3. No model developed in a particular coastal environment/s can be expected to cover all possible beach morphologies. However, by integrating models developed for sites in disparate locations such as the UK, Australia and now the northern coast of Ireland, we can work towards a more comprehensive model. As mentioned previously, Fig. 3 illustrates models based on single barred WD beach, with double and multi-bar beach models required to account for the role and behaviour of the outer bars in their sequential changes, as reviewed by Price et al. (2014). Finally, as the single and multi-bar models apply to unconstrained beaches, modifications to these models are required when constrained by geology and

structures as described by Gallop et al. (2020). This implies a suite of models are required to cover all beach systems, both unconstrained single and double/multi-bar systems, and the impact on these by longshore and cross-shore geological constraints.

6. Conclusions

The northern coast of Ireland was found to have the full range of beach types (WD, TM and TD) and wide spectrum of beach states, reflecting the range in wave and tide conditions around the coast. Observed beach type and state for 95 beaches was obtained from field observations and inspection of satellite and aerial imagery. The role of waves, tides and sediment in this distribution was assessed by predicting beach type using H_b and T_p for a subset of 29 beaches using detailed wave modelling with SWAN to generate H_b and associated T_p, together with modelled tide range and sediment characteristics. The larger sample provided a clear trend in tide range with all WD beach having a TR < 2.1 m, the TM between 2.2 and 3.8 m, and the TD extending from 3 to 3.8 m. Within the 29 subset the increase in tide range between WD,
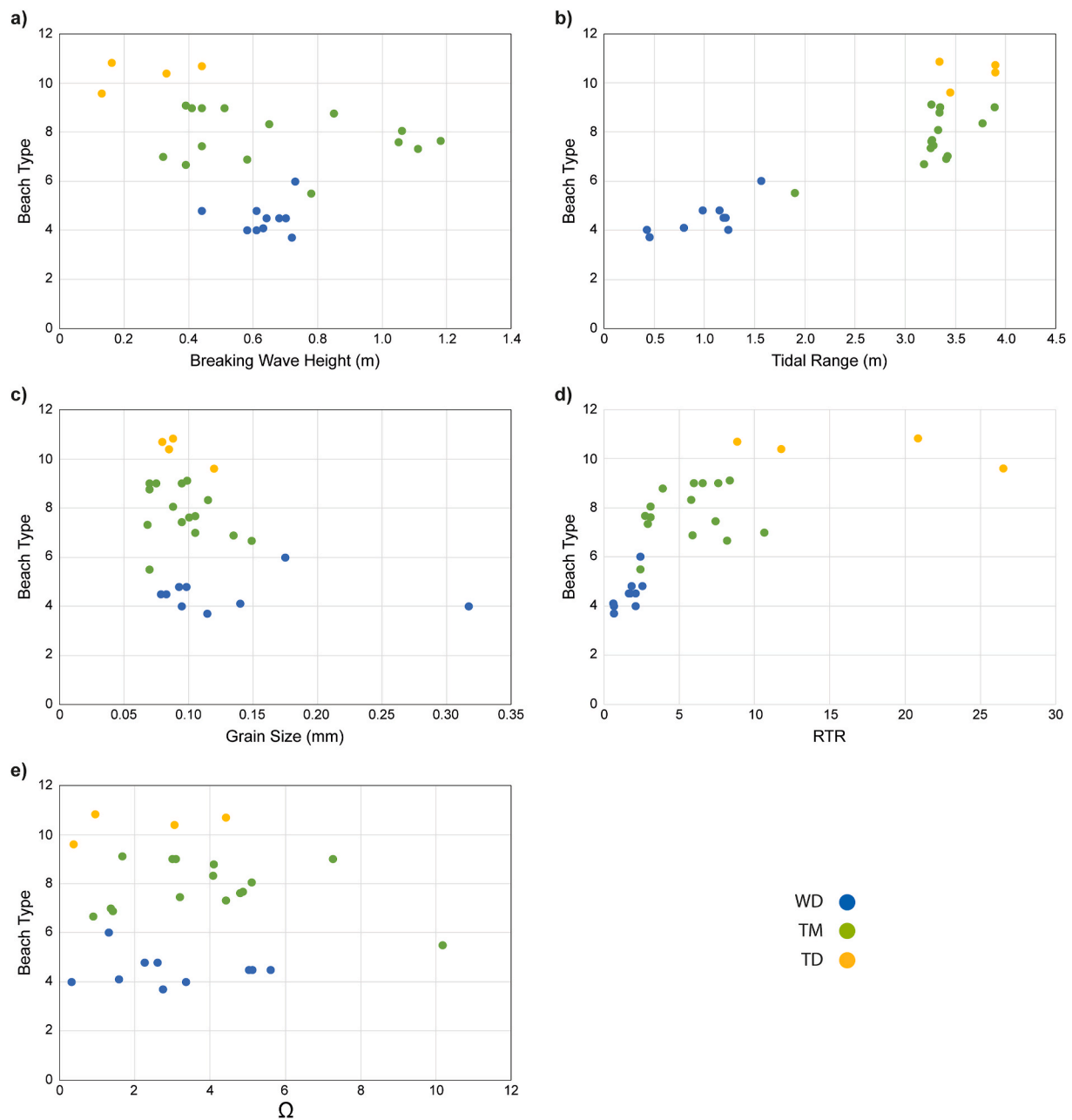
Fig. 8. Beach state for the 29 selected beaches versus **a)** predicted H_b; **b)** spring tide range; **c)** grain size; **d)** predicted RTR; and **e)** predicted Ω. (WD: Wave-Dominated; TM: Tide-Modified; TD: Tide-Dominated).

TM and TD is even better defined and three types agreed well with the RTR boundaries of WD > 3 TM > 10 TM. The beaches were classified using two existing beach models which indicate the need to work towards a unified comprehensive model or beach types and states.

The predicted beach states resided well within the RTR boundaries but were more variable within each WD, TM and TD domain, which may be attributed in part to the sample size and accuracy of both sediment size and predicted H_b. However, the marked improvement in prediction of beach type and state using nearshore wave modelling with SWAN for determining H_b over previous work using simplistic predictions of H_b, highlights the need for accurate measures of all variables, particularly of H_b which is the most difficult to estimate and predict. It also highlights the advantage of using numerical wave modelling in deriving accurate predictions of breaking wave conditions where deepwater wave parameters and detailed nearshore bathymetry are available.

CRediT authorship contribution statement

D.W.T. Jackson: Conceptualization, Data curation, Formal analysis, Funding acquisition, Investigation, Methodology, Supervision, Validation, Visualization, Writing – original draft, Writing – review & editing. **A.D. Short:** Writing – review & editing, Writing – original draft, Methodology, Formal analysis, Conceptualization. **C. Loureiro:** Formal analysis, Methodology, Software, Writing – review & editing, Conceptualization. **J.A.G. Cooper:** Writing – review & editing.

Declaration of competing interest

The authors declare that they have no known competing financial interests or personal relationships that could have appeared to influence the work reported in this paper.

Acknowledgments

References

Anfuso, G., Loureiro, C., Taaouati, M., Smyth, T.A.G., Jackson, D.W.T., 2020. Spatial variability of beach impact from post-tropical cyclone Katia (2011) on Northern Ireland's north coast. Water 12 (5). https://doi.org/10.3390/w12051380.

Anthony, E., 1998. Sediment-wave parametric characterization of beaches. J. Coast Res. 14, 347–352.

Biausque, M., Guisado-Pintado, E., Grottoli, E., Jackson, D.W.T., Cooper, J.A.G., 2021. Seasonal morphodynamics of multiple intertidal bars (MITBs) on a meso- to macrotidal beach. Earth Surf. Process. Landforms. https://doi.org/10.1002/esp.5288.

Booij, N., Holthuijsen, L., Ris, R.C., 1996. The "SWAN" wave model for shallow water. In: Proceedings of the 25th International Coastal Engineering Conference, 1. ASCE, pp. 668–676, 25.

Booij, N., Ris, R.C., Holthuijsen, L.H., 1999. A third-generation wave model for coastal regions, Part I, Model description and validation. J. Geophys. Res. C4 (104), 7649–7666.

Bowden, R., Orford, J.D., 1984. Residual sediment cells on the morphologically irregular coastline of the Ards Peninsula, northern Ireland. Proc. Roy. Ir. Acad. B Biol. Geol. Chem. Sci. 84B, 13–27.

Caballero, I., Stumpf, R.P., 2021. On the use of Sentinel-2 satellites and lidar surveys for the change detection of shallow bathymetry: the case study of North Carolina inlets. Coast. Eng. 169, 103936.

Carter, R.W.G., 1975. Recent changes in the coastal geomorphology of the Magilligan Foreland, Co. Londonderry. In: Proceedings of the Royal Irish Academy, 75B, p. 469497.

Carter, R.W.G., 1979. Recent progradation of the Magilligan foreland, Co. Londonderry, northern Ireland. Actes de Colloques, Centre Nationale and Exploration des Oceans 9, 17–27.

Carter, R.W.G., 1980a. Longshore variations in nearshore wave processes at Magilligan point, Northern Ireland. Earth Surf. Process. 5, 81–89.

Carter, R.W.G., 1980b. Vegetation stabilization and slope failure on eroding sand dunes. Biol. Conserv. 18, 117–122.

Carter, R.W.G., 1986. The morphodynamics of beach-ridge formation, Magilligan, Northern Ireland. Mar. Geol. 73, 191–214.

Carter, R.W.G., 1988. Coastal Environments. Academic Press, London, p. 617.

Carter, R.W.G., 1991. Shifting Sands: A Study of the Coast of Northern Ireland from Magilligan to Larne. HMSO, Belfast., ISBN 0337082537, p. 49

Carter, R.W.G., Lowry, P., Stone, G.W., 1982. Sub-tidal ebb-shoal control of shoreline erosion via wave refraction, Magilligan foreland, Northern Ireland. Mar. Geol. 48, M17–M25.

Carter, R.W.G., Stone, G.W., 1989. Mechanisms associated with the erosion of sand dune cliffs, Magilligan, Northern Ireland. Earth Surf. Process. Landforms 14, 1–10.

Castelle, B., Bonneton, P., Diupuis, H., Sénéchal, N., 2007. Double bar dynamics on the high energy meso-macrotidal French Aquitanian coast: a review. Mar. Geol. 245, 141–159.

Cooper, J.A.G., Navas, F., 2004. Natural bathymetric change as a control on century-scale shoreline behaviour. Geology 32 (6), 513–516.

Cooper, J.A.G., 2007. Geomorphology of Irish estuaries: inherited and dynamic controls. J. Coast. Res. 39, 176–180. SI.

Cooper, J.A.G., 2010. Northern Ireland. In: Bird, E.C.F. (Ed.), Encyclopedia of the World's Coastal Landforms. Springer-Verlag Berlin, pp. 536–544.

Davidson, M.A., Lewis, R.P., Turner, I.L., 2010. Forecasting seasonal to multi-year shoreline change. Coast. Eng. 57, 620–629. https://doi.org/10.1016/j.coastaleng.2010.02.001.

Dee, P., Uppala, S., Simmon, A., et al., 2011. The ERA-Interim reanalysis: configuration and performance of the data assimilation system. Q. J. R. Meteorol. Soc. 137, 553–597.

EMODnet Bathymetry Consortium, 2018. EMODnet Digital Bathymetry (DTM). https://doi.org/10.12770/18ff0d48-b203-4a65-94a9-5fd8b0ec35f6.

Flemming, B.W., Thum, A.B., 1978. The settling tube – a hydraulic method for the grain size analysis of sand. Kiel. Meeresforsch. Sonderh. 4, 82–95.

Gallagher, S., Tiron, R., Dias, F., 2014. A long-term nearshore wave hindcast for Ireland. Atlantic and Irish Sea coasts (1979-2012). Ocean Dynam. 64, 1163–1189. https://doi.org/10.1007/s10236-014-0728-3.

Gallop, S.L., Kennedy, D.M., Loureiro, C., Naylor, L.A., Muñoz-Pérez, J.J., Jackson, D.W.T., Fellows, T., 2020. Geologically controlled sandy beaches: their geomorphology, morphodynamics and classification. Sci. Total Environ. 731, 139123.

Guisado-Pintado, E., Jackson, D.W.T., 2018. Multi-scale variability of Storm Ophelia 2017: the importance of synchronised environmental variables in coastal impact. Sci. Total Environ. 630, 287–301.

Guisado-Pintado, E., Jackson, D.W.T., 2019. Coastal impact from high-energy events and the importance of concurrent forcing parameters: the cases of storm Ophelia (2017) and storm Hector (2018) in NW Ireland. Front. Earth Sci. 7 https://doi.org/10.3389/feart.2019.00190.

Guisado-Pintado, E., 2020. Shallow water wave modelling in the nearshore (SWAN). In: Jackson, D.W.T., Short, A.D. (Eds.), Sandy Beach Morphodynamics. Elsevier, Amsterdam, pp. 391–419.

Harley, M.D., Turner, I.L., Morris, B.D., Short, A.D., Ranasinghe, R., 2007. Nearshore wave climate and localised erosion during high wave events - SE Australia. In: Proc. 18th Australasian Coastal Ocean Engineering Conf. IEAust. Melbourne, Australia (No. 89 CD-ROM).

Hasselmann, K., Barnett, T.P., Bows, E., Carlson, H., Cartwright, D.E., Enke, K., Ewing, J. A., Gienapp, H., Hasselmann, D.E., Kruseman, P., Meerburg, A., Müller, P., Olbers, D. J., Richter, K., Sell, W., Walden, H., 1973. Measurements of wind–wave growth and swell decay during the joint north sea wave project (JONSWAP). Ergänzungsheft zur Deutschen Hydrographischen Zeits A8 (12), 1–95.

Hegge, B., Eliot, I., Hsu, J., 1996. Sheltered sandy beaches of southwestern Australia. J. Coast Res. 12, 748–760.

Holthuijsen, L.H., 2007. Waves in Oceanic and Coastal Waters. Cambridge University Press, Cambridge.

Huang, J., Jackson, D.W.T., Cooper, J.A.G., 2002. Morphological monitoring of a high energy beach system using GPS and total station techniques, Runkerry, County Antrim, Northern Ireland. J. Coast. Res. 36, 390–398. SI.

Jackson, D.W.T., Cooper, J.A.G., Del Rio, L., 2005. Geological control on beach state. Mar. Geol. 216, 297–314.

Jackson, D.W.T., Cooper, J.A.G., 2009a. Application of the equilibrium planform concept to natural beaches in Northern Ireland. Coast. Eng. 57, 112–123.

Jackson, D.W.T., Cooper, J.A.G., 2009b. Geological control on beach form: accommodation space and contemporary dynamics. J. Coast. Res. 56, 69–72. SI.

Jackson, D.W.T., Cooper, J.A.G., O'Connor, M., Guisado-Pintado, E., Loureiro, C., Anfuso, G., 2016. Field measurements of intertidal bar evolution on a high-energy beach system. Earth Surf. Process. Landforms 41 (8), 1107–1114.

Jackson, D.W.T., Short, A.D. (Eds.), 2020. Sandy Beach Morphodynamics. Elsevier, Amsterdam, p. 793.

Klein, A.H.F., Menezes, J.T., 2001. Beach morphodynamics and profile sequence for a headland bay coast. J. Coast Res. 17, 812–835.

Komar, P.D., 1998. Beach Processes and Sedimentation, second ed. Prentice-Hall, p. 544.

Komar, P.D., Gaighan, M.K., 1972. Airy wave theory and breaker height prediction. In: Proc. 13th Coastal Engineering Conference. ASCE, pp. 405–418.

Larson, M., Hoan, L.X., Hanson, H., 2010. Direct formula to compute wave height and angle at incipient breaking. J. Waterw. Port, Coast. Ocean Eng. 136, 119–122.

Levoy, F., Anthony, E.J., Monfort, O., Larsonneur, C., 2000. Morphodynamics of megatidal beaches in Normandy, France. Mar. Geol. 171, 39-39.

Loureiro, C., Cooper, J.A.G., 2020. Temporal variability in winter wave conditions and storminess in the northwest of Ireland. Ir. Geogr. 51, 155–170.

Loureiro, C., Ferreira, Ó., Cooper, J.A.G., 2012. Extreme erosion on high-energy embayed beaches: influence of megarips and storm grouping. Geomorphology 139–140, 155–171.

Loureiro, C., Ferreira, Ó., Cooper, J.A.G., 2013. Applicability of parametric beach morphodynamic state classification on embayed beaches. Mar. Geol. 346, 153–164.

Masselink, G., Short, A.D., 1993. The effect of tide range on beach morphodynamics and morphology: a conceptual model. J. Coast Res. 9, 785–800.

Matias, A., Carrasco, A.R., Loureiro, C., Masselink, G., Andriolo, U., McCall, R., Ferreira, O., Plomaritis, T.A., Pacheco, A., Guerreiro, M., 2019. Field measurements and hydrodynamic modelling to evaluate the importance of factors controlling overwash. Coast. Eng. 152, 103523.

Orford, J.D., 1989. A review of tides, currents and waves in the Irish Sea. In: Sweeney, J. (Ed.), The Irish Sea: A Resource at Risk, Special Publication Number 3. Geographical Society of Ireland, Dublin, pp. 18–46.

Pacheco, A., Horta, J., Loureiro, C., Ferreira, Ó., 2015. Retrieval of nearshore bathymetry from Landsat 8 images: a tool for coastal monitoring in shallow waters. Remote Sens. Environ. 159, 102–116.

Perez, J., Menendez, M., Losada, I.J., 2017. GOW2: a global wave hindcast for coastal applications. Coast. Eng. 124, 1–11.

Pereira, L.C.C., Vila-Concejo, A., Short, A.D., 2016. Coastal morphodynamics processes on the macro-tidal beaches of Pará state under tidally-modulated wave conditions. In: Short, A.D., Klein, A.H.F. (Eds.), Brazilian Beach Systems, vol. 17. Springer, Coastal Research Library, Switzerland, pp. 95–124. https://doi.org/10.1007/978-3-319-30394-9_4.

Price, T.D., Ruessink, B.G., Castelle, B., 2014. Morphological coupling in multiple sandbar systems – a review. Earth Surf. Dyn. 2, 309–321. https://doi.org/10.5194/esurf-2-309-2014.

Proudman Oceanographic Laboratory (POL), 2004. POLPRED for Windows User Guide, p. 62.

Ris, R.C., Booij, N., Holthuijsen, L.H., 1999. A third-generation wave model for coastal regions, Part II, Verification. J. Geophys. Res. C4 (104), 7667–7681.

Ruessink, B.G., van Enckevort, I.M.J., Kingston, K.S., Davidson, M.A., 2000. Analysis of observed two- and three-dimensional nearshore bar behaviour. Mar. Geol. 169, 161–183.

Salmon, J., Holthuijsen, L., 2015. Modeling depth-induced wave breaking over complex coastal bathymetries. Coast. Eng. 105, 21–35.

Saulter, A., 2009. National Centre for Ocean Forecasting Model and Analysis Products Assessment Document. Met Office, p. 95. Unpublished Report.

Scott, T., Masselink, G., Russell, P., 2011. Morphodynamic characteristics and classification of beaches in England and Wales. Mar. Geol. 286, 1–20.

Short, A.D., 1992. Beach systems of the central Netherlands coast: processes and morphology and structural impacts in a storm-driven multi-bar system. Mar. Geol. 107, 103–137.

Short, A.D., 1999. Wave-dominated beaches. In: Short, A.D. (Ed.), Beach and Shoreface Morphodynamics. John Wiley and Sons, Chichester, pp. 173–203.

Short, A.D., 2006. Australian beach systems – nature and distribution. J. Coast Res. 22, 11–27.

Short, A.D., 2020. Wave-dominated, tide-modified and tide-dominated beach continuum. In: Jackson, D.W.T., Short, A.D. (Eds.), Sandy Beach Morphodynamics. Elsevier, Amsterdam, pp. 363–390.

Short, A.D., Aagaard, T., 1993. Single and multi-bar beach model. J. Coast. Res. 15, 141–157. SI.

Short, A.D., Jackson, D.W.T., 2013. Beach morphodynamics. In: Shroder, J.F. (Ed.), Treatise in Geomorphology, vol. 10. Academic Press, San Diego.

Sinnot, A.M., Devoy, R.J.N., 1992. The geomorphology of Ireland's coastline: patterns, processes and future prospects. In: Hommes et Terres du Nord, pp. 145–153. https://doi.org/10.3406/htn.1992.2370, 1992/3. Les littoraux.

Sunamura, T., 1984. T. Quantitative predictions of beach-face slopes. Geol. Soc. Am. Bull. 95, 242–245.

Turner, J.F., Iliffe, J.C., Ziebart, M.K., Wilson, C., Horsburgh, K.J., 2010. Interpolation of tidal levels in the coastal zone for the creation of a hydrographic datum. J. Atmos. Ocean. Technol. 27, 605–613.

Traganos, D., Poursanidis, D., Aggarwal, B., Chrysoulakis, N., Reinartz, P., 2018. Estimating satellite-derived bathymetry (SDB) with the Google Earth engine and Sentinel-2. Rem. Sens. 10, 859.

Vital, H., Silveira, I.M., Tabosa, W.F., Lima, Z.M.C., Pinheiro Lima Filho, F., Souza, F.E.S., Chaves, M.S., Pimenta, F.M., Gomes, M.P., 2016. Beaches of Rio Grande do Norte. In: Short, A.D., Klein, A.H.F. (Eds.), Brazilian Beach Systems, vol. 17. Springer, Coastal Research Library, Switzerland, pp. 95–124. https://doi.org/10.1007/978-3-319-30394-9_8.

Wright, L.D., Short, A.D., 1984. Morphodynamic variability of surf zones and beaches: a synthesis. Mar. Geol. 56, 93–118.

Wright, L.D., Short, A.D., Green, M.O., 1985. Short term changes in the morphodynamic states of beaches and surf zones: an empirical predictive model. Mar. Geol. 62, 339–364.